Journal of Materials Chemistry A

PAPER

View Article Online
View Journal | View Issue

Cite this: J. Mater. Chem. A, 2014, 2, 1006

Promoting long-term cycling performance of high-voltage Li_2CoPO_4F by the stabilization of electrode/electrolyte interface†

Xiaobiao Wu,[a] Sihui Wang,[a] Xiaochen Lin,[a] Guiming Zhong,[a] Zhengliang Gong[b] and Yong Yang*[ab]

Received 22nd September 2013
Accepted 28th October 2013

DOI: 10.1039/c3ta13801a

www.rsc.org/MaterialsA

High-voltage Li_2CoPO_4F (~5 V *vs.* Li/Li^+) with double-layer surface coating has been successfully prepared for the first time. The Li_3PO_4-coated Li_2CoPO_4F shows a high reversible capacity of 154 mA h g^{-1} (energy density up to 700 W h kg^{-1}) at 1 C current rate, and excellent rate capability (141 mA h g^{-1} at 20 C). XRD and MAS NMR results show that Li_2CoPO_4F can be indexed as an orthorhombic structure with space group *Pnma* and coexists with Li_3PO_4. The XPS depth profiles and TEM analysis reveal that the as-prepared material has a double-layer surface coating, with a carbon outer layer and a Li_3PO_4 inner layer, which greatly enhances the transfer kinetics of the lithium ions and electrons in the material and stabilizes the electrode/electrolyte interface. Using LiBOB as an electrolyte additive is another way to further stabilize the electrode/electrolyte interface, and the LiBOB has a synergistic effect with the Li_3PO_4 coating layer. In this way, the Li_2CoPO_4F cathode material exhibits excellent long-term cycling stability, with 83.8% capacity retention after 150 cycles. The excellent cycling performance is attributed to the LiBOB electrolyte additive and the Li_3PO_4 coating layer, both of which play an important role in stabilizing the charge transfer resistance of Li_2CoPO_4F upon cycling.

Introduction

Lithium ion batteries are regarded as a promising power source for electric vehicles (EV) and hybrid electric vehicles (HEV). However, current Li-ion battery technology cannot meet the demands of large-scale application yet, partially due to its low energy density. Therefore, there is a great demand for developing new materials with high energy density and high power density, especially cathode materials.[1] Recently, fluorophosphates have been widely investigated as a new kind of polyanion cathode material.[2–7] The combination of the inductive effect of the PO_4^{3-} group and the high electronegativity of the F^- anion makes fluorophosphates promising cathode materials with high working voltages. Additionally, introducing the F^- anion allows fluorophosphates to exchange two electrons per formula unit, thus achieving high capacity. Li_2CoPO_4F can be regarded as one of the most attractive cathode materials among the fluorophosphates. Density functional theory (DFT) calculation results show that $Li_2CoPO_4F/LiCoPO_4F$ and $LiCoPO_4F/CoPO_4F$ have average open circuit voltages of 4.8 V and 5.2 V, respectively.[8] Furthermore, a high theoretical capacity of 287 mA h g^{-1} can be achieved for Li_2CoPO_4F, supposing that two lithium ions can be reversibly utilized per formula unit. Therefore, Li_2CoPO_4F is a promising high energy density cathode material with a theoretical energy density of about 1435 W h kg^{-1}, which is much higher than that of commercial cathode materials such as $LiCoO_2$ (theoretical/practical: ~1068/546 W h kg^{-1}), $LiFePO_4$ (theoretical/practical: ~578/578 W h kg^{-1}) and $LiMn_2O_4$ (theoretical/practical: ~593/480 W h kg^{-1}).

Many efforts have been devoted to the synthesis and improvement of the electrochemical properties of Li_2CoPO_4F. Nevertheless, Li_2CoPO_4F often suffers from fast capacity fading, which results from the serious decomposition of the electrolyte at high working voltage and the catalytic effect of cobalt.[9,10] In our previous study, we used the sol–gel method to synthesize a Li_2CoPO_4F/C nanocomposite with high capacity and excellent rate performance. Unfortunately, Li_2CoPO_4F also suffers from poor cycling performance.[11] Recently, Xu *et al.* investigated the stability of conventional carbonate-based solvent on $LiNi_{0.45}Cr_{0.05}Mn_{1.5}O_4$.[12] Their results indicate that the stability of the electrolyte strongly depends on the properties of the cathode materials. The catalytic effect of cobalt also results in the serious decomposition of the electrolyte at high voltage.[13] Therefore, the cycling performance of the materials can be improved by regulating the surface properties of cathode materials, through surface modification of the active materials and/or using a film-forming electrolyte additive. Metal oxides,

[a]State Key Laboratory of Physical Chemistry of Solid Surfaces, Department of Chemistry, College of Chemistry and Chemical Engineering, Xiamen University, Xiamen 361005, P. R. China. E-mail: yyang@xmu.edu.cn

[b]School of Energy Research, Xiamen University, Xiamen 361005, P. R. China

† Electronic supplementary information (ESI) available: Crystal structure, NMR, SEM and electrochemical data. See DOI: 10.1039/c3ta13801a

metal fluorides and metal phosphates have been widely applied to modify the surface of cathodes and thus isolate the active materials from electrolyte.[14–19] However, *in situ* coating of metal-based compounds on the surface of cathode materials is difficult to realize perfectly, because metal ions can easily intercalate into the lattice of cathode materials during high temperature heat treatment. Li_3PO_4 is a fast lithium ionic conductor and has been extensively used as a coating layer to improve the cycling performance of cathode materials.[20–23] Furthermore, fast ionic conductive film coating on the surface can eliminate the surface anisotropy of the active material and therefore enhance the rate capability.[24] Above all, the heat treatment process does not introduce extra chemical elements into Li_3PO_4, which can avoid the structural degradation of the pristine sample. Therefore, the *in situ* coating of Li_3PO_4 can be successfully achieved. Using a film-forming electrolyte additive is also an effective way to form a stable interface between the active material and the electrolyte on the electrode surface.[25–27] Lithium bis(oxalate)borate (LiBOB) electrolyte additive has been successfully used in high voltage cathode materials to improve the capacity retention upon cycling.[27–29] It is thought that the oxidation product of LiBOB on the electrode surface can, at the same time, generate a passive film to further restrict decomposition of the electrolyte.

In this study, the combination of Li_3PO_4 coating and LiBOB electrolyte additive is applied to improve the cycling performance of Li_2CoPO_4F. We use a sol–gel method to synthesize $Li_2CoPO_4F/Li_3PO_4/C$ nanocomposite with a unique double-layer surface coating. The rate capability and cycling performance are significantly improved. Having a synergistic effect with the Li_3PO_4 coating layer, the LiBOB electrolyte additive is also adopted to further enhance the cycling performance.

Experimental

Materials synthesis

Li_2CoPO_4F was synthesized by a sol–gel method as previously reported.[11] The Li_3PO_4-coated sample was synthesized by adding excess amounts of LiF and H_3PO_4. In brief, for the Li_3PO_4-coated sample, 0.01 mol $Co(NO_3)_2 \cdot 6H_2O$, 0.02 mol citric acid, 0.0275 mol LiF and 0.0125 mol H_3PO_4 (85 wt% solution) were dissolved in 50 mL deionized water under vigorous stirring at 80 °C for 24 h to form a dark red solution. 1.8 mL ethylene glycol was added to the above solution, and then the solution was continuously stirred for a further 2 h at 120 °C. The resulting solution was dried at 100 °C in an oven to obtain the precursor. The precursor was ground and pelletized, then heat-treated at 600 °C in a tubular furnace under an argon atmosphere for 6 h. The redundant fluorine was removed in the form of exhaust.[30] Excess amounts of LiF and H_3PO_4 are used to achieve the *in situ* Li_3PO_4 coating. The molar ratio of Li_2CoPO_4F to Li_3PO_4 was 4 : 1 for the Li_3PO_4-coated sample. The carbon content was determined using a Vario EL III elemental analyzer (Elementar Analysen System GmbH, Germany). The carbon content was 12.2% for the pristine sample and 11.3% for the Li_3PO_4-coated sample.

Material characterization

X-ray diffraction (XRD) patterns were collected on a Panalytical X-pert diffractometer (PANalytical, Netherlands). Scanning electron microscopy (SEM) images were taken on a S-4800 (HITACHI, Japan) microscope, operating at 20 kV. X-ray photoelectron spectroscopy (XPS) of the samples was measured with a Quantum 2000 ESCA spectrometer (Physical Electronics, USA). Transmission electron microscopy (TEM) and high resolution transmission electron microscopy (HRTEM) analysis were performed on a Tecnai F30 (Philips-FEI, Netherlands) apparatus, operating at 300 kV. The ^{7}Li and ^{31}P MAS NMR experiments were performed on a Bruker Avance 400 NMR spectrometer using a 2.5 mm double-resonance MAS NMR probe with a spinning frequency of 28 kHz. The ^{7}Li spectra were acquired at a Larmor frequency of 155.5 MHz using a small angle pulse length of 0.4 μs and a recycle delay of 15 s. The spectra were referenced to LiCl powder (0 ppm). The ^{31}P spectra were acquired at a Larmor frequency of 162.0 MHz using a small angle pulse length of 0.5 μs and a recycle delay of 0.5 s. The spectra were referenced to adenosine diphosphate (ADP) powder (0 ppm).

Electrochemical measurements

The electrochemical performance was measured using CR2025 coin cells. The working electrodes were fabricated from the active material, acetylene black and PVDF at a weight ratio of 70 : 20 : 10 on an aluminum current collector with a diameter of 1.6 cm. The mass of active material loading was controlled to between 2 and 3 mg. Metal lithium was used as the counter electrode. 1 M $LiPF_6$ in EC–DMC (1 : 1, by volume) (reference electrolyte) or the reference electrolyte with 1 wt% LiBOB additive was used as the electrolyte. The coin cells were assembled in an argon-filled glove box. Galvanostatic charge/discharge tests were performed at various n C current rates (1 C = 143 mA g^{-1}) in the voltage range of 2–5.4 V or 2–5.2 V at 30 °C. The capacity was calculated based on the mass of Li_2CoPO_4F. Though inactive carbon and Li_3PO_4 must be considered for practical applications, we only want to evaluate the electrochemical performance of Li_2CoPO_4F in this study, and thus the mass of inactive carbon and Li_3PO_4 are not included in the calculation of the mass of active materials. Electrochemical impedance spectroscopy experiments were carried out on an Autolab workstation (Eco Chemie, Netherlands). The frequency range was from 100 kHz to 10 mHz and the AC perturbation amplitude was ±5 mV. The EIS data were collected at the charged state of 4.9 V.

Results and discussion

Fig. 1a shows the XRD patterns of the pristine and the Li_3PO_4-coated Li_2CoPO_4F samples. It can be seen that the pristine Li_2CoPO_4F sample has a $LiCoPO_4$ impurity phase, which could be due to the relatively low heat treatment temperature.[11,31] However, for the Li_3PO_4-coated sample, the $LiCoPO_4$ impurity disappears. It is speculated that the excess amount of LiF can help to form the pure phase Li_2CoPO_4F. Furthermore, the

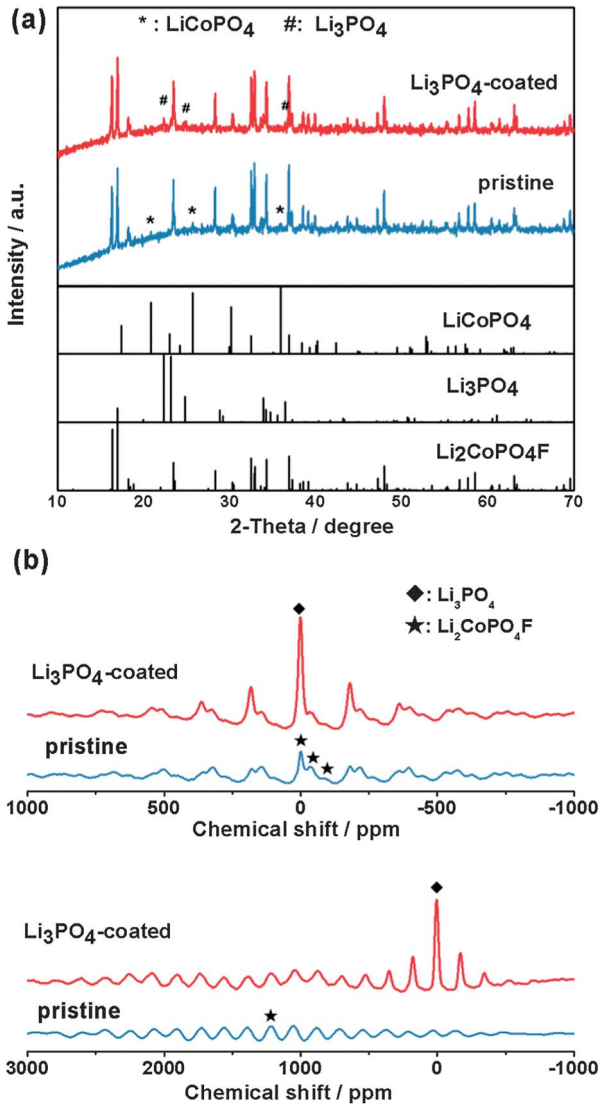

Fig. 1 (a) XRD patterns and (b) ^{7}Li and ^{31}P MAS NMR spectra of the pristine and the Li_3PO_4-coated Li_2CoPO_4F samples. The ^{7}Li chemical shifts are 1.5 ppm for Li_3PO_4, and 1.5 ppm, −32.6 ppm, −81.8 ppm for Li_2CoPO_4F; the ^{31}P chemical shifts are 6.0 ppm for Li_3PO_4, and 1223.1 ppm for Li_2CoPO_4F.

Li_3PO_4 phase can also be detected in the XRD pattern, indicating that Li_3PO_4 co-exists with Li_2CoPO_4F. Except for the peaks of $LiCoPO_4$ and Li_3PO_4, all the diffraction peaks of Li_2CoPO_4F in the pristine and the Li_3PO_4-coated samples can be indexed to an orthorhombic structure with space group *Pnma*. Li_2CoPO_4F is isostructural with Li_2NiPO_4F, and the crystal structure of Li_2CoPO_4F is illustrated in Fig. S1 (see ESI†). The calculated lattice parameters are $a = 10.458$ Å, $b = 6.377$ Å, $c = 10.880$ Å and $V = 725.70$ Å^3 for the pristine sample; $a = 10.460$ Å, $b = 6.378$ Å, $c = 10.883$ Å and $V = 726.17$ Å^3 for the Li_3PO_4-coated sample. Compared with the pristine sample, the lattice parameters of the Li_3PO_4-coated sample do not show obvious changes, indicating that the Li_3PO_4 coating layer does not intercalate into the lattice of Li_2CoPO_4F and does not change the orthorhombic structure of Li_2CoPO_4F.

Fig. 1b shows the ^{7}Li and ^{31}P MAS NMR spectra for the pristine and the Li_3PO_4-coated Li_2CoPO_4F samples. Compared with the pristine sample, the intensity of the chemical shift located at 1.5 ppm for ^{7}Li and 6.0 ppm for ^{31}P are much stronger for the Li_3PO_4-coated sample. Since ^{7}Li (1.5 ppm) and ^{31}P (6.0 ppm) are assigned to Li_3PO_4 (ESI, Fig. S2 and S3†), this result demonstrates that the excess amounts of lithium and phosphate exist in the form of Li_3PO_4, which agrees well with the XRD result.

The SEM images of the pristine and the Li_3PO_4-coated Li_2CoPO_4F samples are shown in Fig. S4a–d (see ESI†). It can be seen that the particle sizes of the two samples are micrometer-scale and are not uniformly distributed. Under high magnification, the primary particle size is only tens of nanometers for both samples. There is no significant difference between the pristine and the Li_3PO_4-coated samples in the SEM images, indicating that the Li_3PO_4 coating does not significantly change the surface morphology of the Li_2CoPO_4F sample. It is necessary to point out that the amount of Li_3PO_4 in our experiment is higher than that reported in the literature.[20,22] Because of the nano-sized primary particles, a large amount of Li_3PO_4 is required to achieve an effective and uniform coating layer (the optimized amount of Li_3PO_4 is shown in Fig. S5, see ESI†).

Fig. 2a shows the atomic percentage and P : F ratio obtained by quantitative analysis of XPS depth profiles of the Li_3PO_4-coated Li_2CoPO_4F sample. Quantitative analysis of the XPS depth profiles indicates that the atomic percentage of carbon obviously decreases from the outside to the inside of the sample, while the atomic percentages of phosphorus and fluorine increase from the outside to the inside. This result indicates that carbon is distributed on the outer layer of the Li_3PO_4-coated Li_2CoPO_4F sample.[32] The ratio of phosphorus to fluorine decreases from the outside to the inside, which indicates that Li_3PO_4 is coated on the surface of Li_2CoPO_4F. The formation of a double-layer surface modified Li_2CoPO_4F sample was further confirmed by HRTEM measurements, as shown in Fig. 2b. The amorphous carbon layer with a thickness of 3–6 nm can be clearly observed in the outer layer. What is more, crystalline Li_3PO_4 with a thickness of 4–6 nm is present in the inner layer. Fast ion conductor coating on the surface of active materials can be realized by *in situ* synthesis methods, as has been reported in the literature.[33,34] In addition, carbon coating in the outer layer can effectively enhance the electronic conductivity and restrict the growth of particle size, while the Li_3PO_4 in the inner layer can isolate the active material from the electrolyte and also improve the ionic conductivity of the electrode materials at the same time. Owing to this double-layer surface modification, greatly improved electrochemical performance of the Li_2CoPO_4F cathode material can be expected.

Fig. 3 shows the first charge/discharge profiles of the Li_2CoPO_4F samples at various current rates. As can be seen, the Li_3PO_4-coated sample in the reference electrolyte (C-R) delivers a reversible capacity as high as 154 mA h g^{-1} at 1 C current rate, which is much higher than that of the pristine sample in the reference electrolyte (P-R). The corresponding energy density is up to 700 W h kg^{-1}, which is higher than that of its analogues: $LiFePO_4$, $LiCoPO_4$ and Li_2FePO_4F, as shown in Fig. 4. It is worth

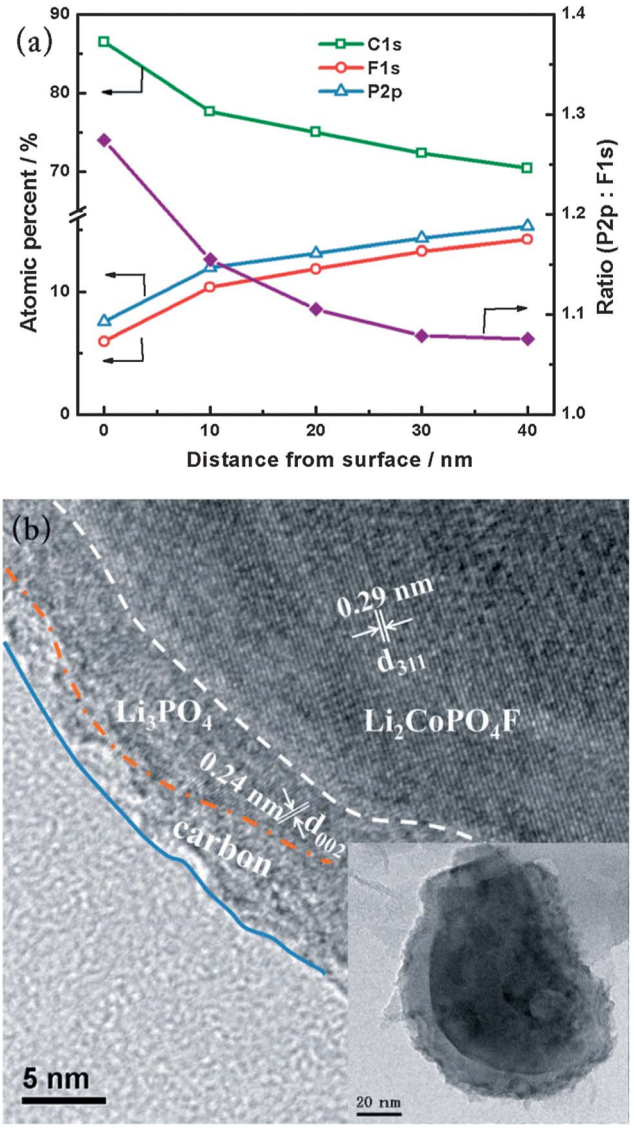

Fig. 2 (a) Atomic percentage and P : F ratio obtained by quantitative analysis of XPS depth profiles of the Li_3PO_4-coated Li_2CoPO_4F sample. (b) HRTEM image of the Li_3PO_4-coated Li_2CoPO_4F sample.

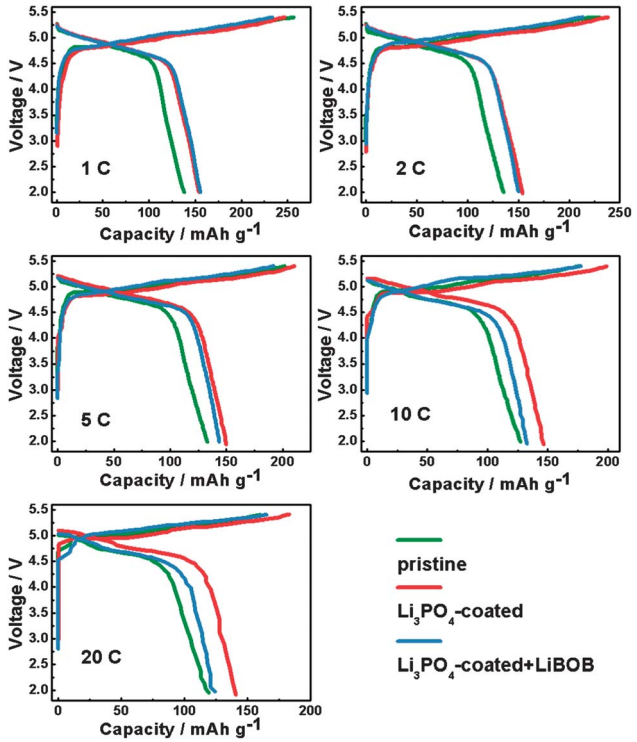

Fig. 3 The first charge/discharge profiles of the Li_2CoPO_4F samples at various rates (1 C = 143 mA g^{-1}).

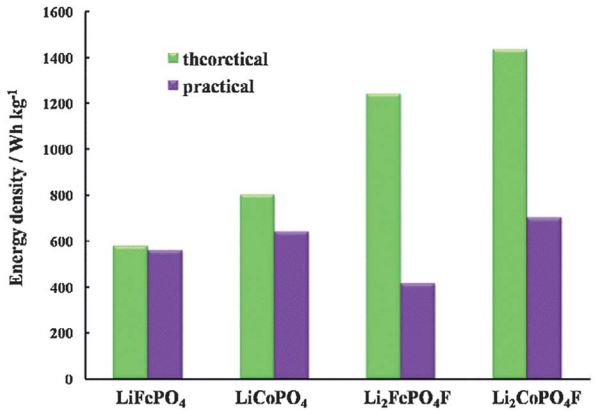

Fig. 4 Comparison of the theoretical and practical energy densities of $LiFePO_4$, $LiCoPO_4$, Li_2FePO_4F and Li_2CoPO_4F.

mentioning that the initial discharge capacity exceeds the theoretical capacity calculated based on one electron exchange per formula unit (143 mA h g^{-1}). The reason for this excess discharge capacity is not clear, and may come from the reversible redox reaction of Co^{3+}/Co^{4+}, and/or PF_6^- anion intercalation/de-intercalation into/out of the carbon.[12,35] Further efforts must be devoted to uncovering the detailed reasons for this (*e.g. in situ* XAS).

When comparing the electrochemical performance of the pristine and the Li_3PO_4-coated samples in the reference electrolyte, it is found that the Li_3PO_4-coated Li_2CoPO_4F sample exhibits outstanding rate performance. Even at 20 C current rate, the Li_3PO_4-coated Li_2CoPO_4F sample in the reference electrolyte can still deliver a discharge capacity of up to 141 mA h g^{-1}, showing 92% capacity retention of that at 1 C current rate. In order to make a clearer comparison, Fig. 5 shows the initial discharge capacities at various rates by normalizing the capacity at 1 C current rate to 100%. It can clearly be seen that the Li_3PO_4-coated sample shows much better rate capability than the pristine sample, especially at high current rates. The Li_3PO_4 coating layer, which reduces the contact area between the Li_2CoPO_4F active material and the electrolyte, can reduce the polarization (the higher midpoint voltage as shown in Fig. 5), and contributes greatly to the impressive rate capability (compared with the pristine sample). On the other hand, the Li_3PO_4 coating layer acts as a good ionic conductor, and can eliminate the anisotropy of the surface properties of the Li_2CoPO_4F cathode material and allow fast

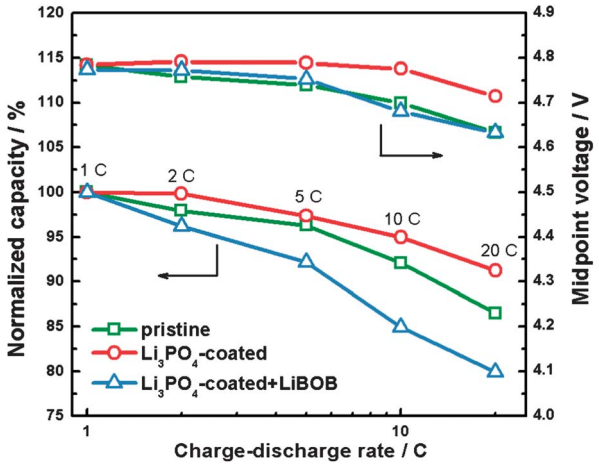

Fig. 5 Comparison of the normalized capacities and midpoint voltages of the Li_2CoPO_4F samples at various rates.

lithium ion diffusion along the preferred orientations, which has been demonstrated by $LiFePO_4$.[24] The lithium ion diffusion coefficient of the Li_3PO_4-coated sample is 4.3 times higher than that of the pristine one (ESI, Fig. S6†). Therefore, the outstanding electrochemical properties (energy density and power density) are ascribed to the unique double-layer surface modification. However, the amount of Li_3PO_4 coating layer should be carefully controlled, because Li_3PO_4 is also a poor electronic conductor and an excessive amount of Li_3PO_4 would affect the rate capability (the electrochemical performance of an excessive amount of Li_3PO_4 is shown in Fig. S7,† the electrochemical impedance results as a function of the Li_3PO_4 amount are shown in Fig. S8, see ESI†).

It has been reported that LiBOB as an electrolyte additive can improve the interfacial properties of cathode materials.[27,36] It can be seen that the Li_3PO_4-coated sample in the electrolyte with LiBOB additive (C-A) delivers a similar first discharge capacity to Li_2CoPO_4F (C-R) at small current density (*e.g.* 1 C and 2 C). However, when the current rate increases, the discharge capacity of Li_2CoPO_4F (C-A) decays more quickly than that of Li_2CoPO_4F (C-R), accompanied by an obvious discharge voltage drop (lower midpoint voltage, as shown in Fig. 5). It is believed that the LiBOB additive helps to from a stable solid electrolyte interface (SEI) layer during the charge/discharge process, which increases the interfacial resistance and affects the rate capability.

Fig. 6 shows the cycling performances of the Li_2CoPO_4F samples at various current rates. It can be seen that Li_2CoPO_4F (P-R) shows poor cycling performance. The fast capacity fading is the result of serious side decomposition of the electrolyte on the surface of Li_2CoPO_4F at high operating voltage.

According to the literature, cobalt-based compounds possess high catalytic activity, which accelerates the decomposition reaction of the electrolyte at high voltage.[12,13] Therefore, if the interfacial properties of Li_2CoPO_4F can be improved by keeping the highly catalytic Li_2CoPO_4F cathode material from direct contact with the electrolyte, the cycling performance should be significantly enhanced.

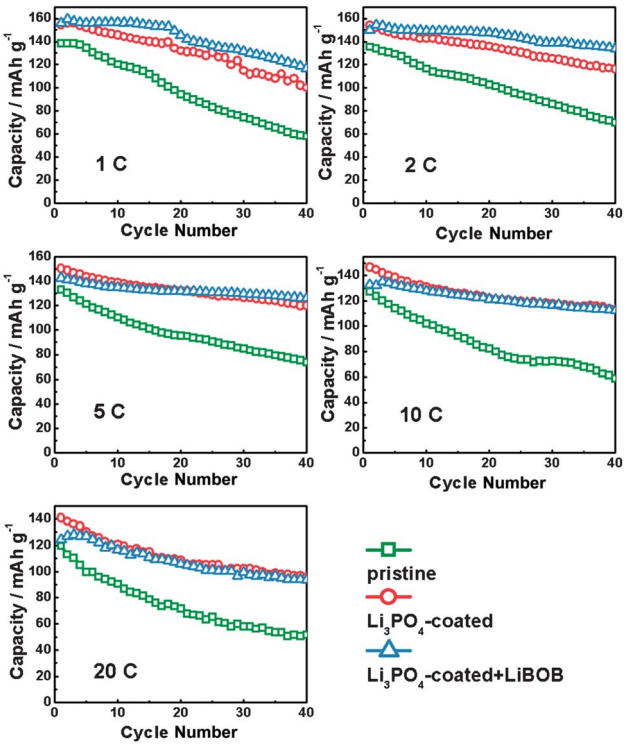

Fig. 6 Cycling performances of the Li_2CoPO_4F samples at various rates.

As shown in Fig. 6, the Li_3PO_4-coated Li_2CoPO_4F exhibits obvious improvement in cycling performance compared with the pristine sample in the reference electrolyte. For example, Li_2CoPO_4F (C-R) shows a discharge capacity of 120 mA h g^{-1} with 79.8% capacity retention after 40 cycles at 5 C current rate, while a capacity of 74 mA h g^{-1} with 55.5% capacity retention after 40 cycles is obtained for the pristine sample. This result indicates that the stability of the interface could be enhanced by the Li_3PO_4 coating, which possesses high chemical resistance and keeps the active material away from the electrolyte. On the other hand, the enhanced diffusion property of lithium ions through the Li_3PO_4 coating may also contribute to the improved cycling performance.

Electrolyte additives are another efficient way to stabilize the electrode/electrolyte interface. This strategy also works efficiently in our Li_2CoPO_4F system. The cycling performances of the Li_3PO_4-coated Li_2CoPO_4F in reference electrolyte and in electrolyte with LiBOB additive are compared at various rates (as shown in Fig. 6). It is clearly shown that LiBOB is an effective electrolyte additive to enhance the cycling performance. After 40 cycles, the capacity retention is 75.5% and 89.3% for the Li_3PO_4-coated Li_2CoPO_4F in reference electrolyte and in electrolyte with additive at 2 C current rate, respectively. It is speculated that the oxidation of LiBOB on the electrode surface can generate a passive film that inhibits progressive damage to the surface structure of the Li_2CoPO_4F cathode material.[36] However, the passive film and the low ionic conductivity of the electrolyte with LiBOB additive would affect the rate capability.[37] The electrochemical performances of the pristine Li_2CoPO_4F in

electrolyte with/without LiBOB additive were also studied, and the results are similar to those of the Li_3PO_4-coated sample (ESI, Fig. S9†). Table 1 summarizes the first cycle discharge capacity, 40th cycle discharge capacity and capacity retention of Li_2CoPO_4F samples at various rates. It can be seen that surface modification has a synergistic effect with the electrolyte additive. The results clearly demonstrate that the surface modification and electrolyte additive contribute greatly to the stability of the interface between the electrode and electrolyte. Comparing with the initial coulombic efficiencies for the Li_2CoPO_4F samples (P-R, C-R and C-A) at various rates, we also reach the same conclusion (ESI, Table S1†).

EIS is used to better understand the reasons why the cycling performances of the Li_3PO_4-coated Li_2CoPO_4F in the reference electrolyte and in the electrolyte with LiBOB additive have been improved greatly. Fig. 7 shows the Nyquist plots of the Li_2CoPO_4F samples (P-R, C-R and C-A) after 10, 20, 30 and 40 cycles. The data were collected at the charged state of 4.9 V. Generally speaking, the high frequency semicircle region is related to lithium ion diffusion in the solid electrolyte interface (SEI) and coating layer (R_f), the middle frequency semicircle region is related to the charge transfer resistance (R_{ct}) between the active material and the surface film, and the low frequency slope region represents lithium ion diffusion in the bulk material. It can be clearly seen that the R_f after 10 cycles increases in the order: P-R < C-R < C-A, while the R_{ct} after 10 cycles shows the opposite trend. The diffusion of lithium ions in the coating layer results in the R_f of C-R being larger than that of P-R. Compared with the C-R sample, the larger R_f of the C-A sample could be due to the stable interface film on the electrode surface caused by the oxidation of the LiBOB additive upon cycling. This larger interface resistance reduces the rate capability of the Li_3PO_4-coated Li_2CoPO_4F sample in the electrolyte with additive compared with the reference electrolyte. Interestingly, the surface modification effectively suppresses the growth rate of R_{ct} during cycling, and in the meantime the electrolyte additive can further stabilize the R_{ct}. The relatively stable charge transfer resistance upon cycling makes the C-A sample exhibit good cycling performance. The surface modification and film-forming electrolyte additive contribute a lot to the formation of a stable electrode/electrolyte interface film, thus reducing the contact area between active material and electrolyte as well as suppressing the increase in charge transfer resistance. Therefore, the poor cycling performance is mainly due to the deterioration of the electrode/electrolyte interface rather than structural changes. If a stable interface layer is formed, the cycling performance of Li_2CoPO_4F can be significantly improved.

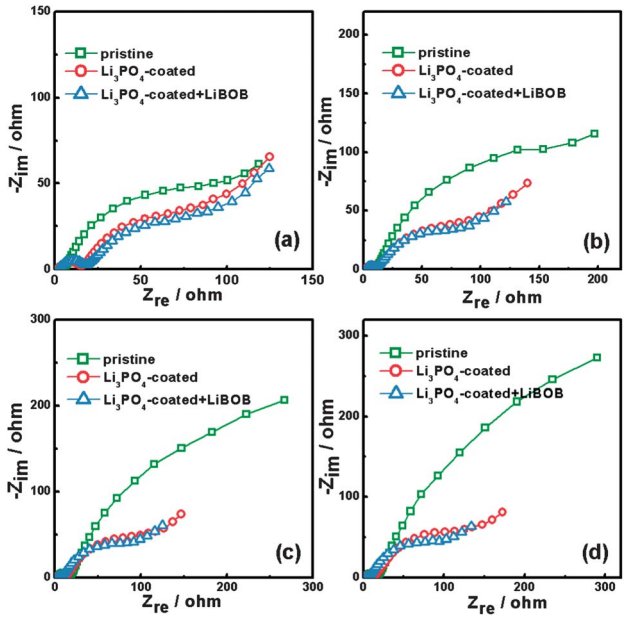

Fig. 7 Nyquist plots of the Li_2CoPO_4F samples after (a) 10 cycles, (b) 20 cycles, (c) 30 cycles and (d) 40 cycles. The data were collected at the charged state of 4.9 V.

In order to investigate the function of the LiBOB additive, XPS was used to determine the surface composition of the Li_3PO_4-coated Li_2CoPO_4F electrode before cycling, after one cycle in the reference electrolyte and in the electrolyte with additive. The XPS spectra of the surface of fresh and cycled Li_3PO_4-coated Li_2CoPO_4F electrodes are shown in Fig. 8. The peak at 781.7 eV in the spectra is assigned to Co^{2+} in Li_2CoPO_4F. After one cycle in the reference electrolyte and in the electrolyte with additive, the peak at 781.7 eV disappears, indicating that the surface of the Li_2CoPO_4F electrode is covered with the decomposition product of the electrolyte. The intensity of the peak at 56.0 eV (assigned to the Li 1s in LiF)[38] increases in the order: fresh electrode < electrode cycled in electrolyte with

Table 1 The first cycle discharge capacities, 40th cycle discharge capacities and capacity retention of the Li_2CoPO_4F samples at various rates in the voltage range of 2–5.4 V

	Pristine			Li_3PO_4-coated			Li_3PO_4-coated + LiBOB		
Current rate	1st cycle capacity (mA h g^{-1})	40th cycle capacity (mA h g^{-1})	Capacity retention (%)	1st cycle capacity (mA h g^{-1})	40th cycle capacity (mA h g^{-1})	Capacity retention (%)	1st cycle capacity (mA h g^{-1})	40th cycle capacity (mA h g^{-1})	Capacity retention (%)
1 C	138	58	42.0	154	100	65.0	156	117	75.0
2 C	135	70	51.6	154	116	75.5	150	134	89.3
5 C	133	74	55.5	150	120	79.8	142	126	88.7
10 C	127	59	46.3	146	113	77.4	132	113	85.6
20 C	119	52	43.2	141	96	68.1	125	94	75.2

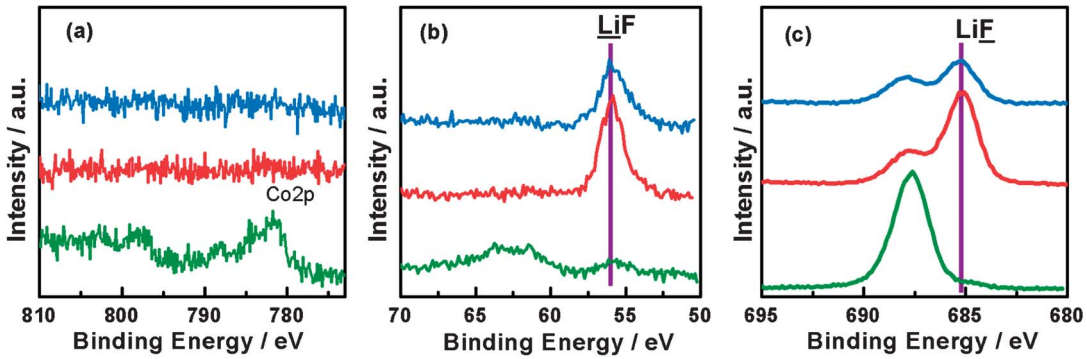

Fig. 8 XPS spectra of the surface of the Li_3PO_4-coated Li_2CoPO_4F electrode before cycling (green line), after one cycle in reference electrolyte (red line) and after one cycle in electrolyte with LiBOB additive (blue line): (a) Co2p, (b) Li1s, (c) F1s.

LiBOB additive < electrode cycled in reference electrolyte. This phenomenon is attributed to the decomposition products of the electrolyte that covered the electrode surface. However, a stable interface film formed during the charge/discharge process as the result of the LiBOB additive can reduce the contact area of the electrode/electrolyte interface and cause a smaller amount of decomposition products to cover the surface. The analysis of the XPS F 1s spectrum also gives a similar result. As a poor Li^+ ion and electronic conductor, LiF covering the electrode surface would significantly increase the charge transfer resistance upon cycling.[19,39] Therefore, the LiBOB additive helps to form a stable interface film that can stabilize the charge transfer resistance upon cycling.

Recently, Xu *et al.* have reported that the conventional carbonate-based solvent is stable up to 5.2 V on spinel cathode material $LiNi_{0.45}Cr_{0.05}Mn_{1.5}O_4$.[12] The stability of the conventional electrolyte depends on the surface property of cathode material. The surface modification and film-forming electrolyte additive can effectively improve the surface property of a cathode material. Therefore, the Li_3PO_4-coated Li_2CoPO_4F cathode material was cycled in the voltage range of 2–5.2 V in the electrolyte with LiBOB additive to study the long-term cycling performance. Fig. 9 shows the cycling performance of the Li_3PO_4-coated Li_2CoPO_4F in the electrolyte with LiBOB additive in the voltage range of 2–5.2 V at a current density of 143 mA g^{-1}. As can be seen, the Li_2CoPO_4F cathode material can deliver a reversible discharge capacity of 136 mA h g^{-1} at the first cycle, and the capacity gradually increases to its maximum value of 142 mA h g^{-1} at the fifth cycle. Decreasing the upper cut-off voltage limit does not significantly affect the discharge capacity at 1 C current density. A capacity of 119 mA h g^{-1} with a capacity retention of 83.8% (*versus* maximum capacity) is achieved after 150 cycles. To the best of our knowledge, this is the first report of the long-term cycling performance of a Li_2CoPO_4F cathode material. The capacity decay is mainly concentrated in the first 35 cycles, while the capacity decay is only 10 mA h g^{-1} over the next 115 cycles. This result demonstrates that a stable interface film formed during the first several cycles can effectively improve the interfacial properties of electrode. It can be seen from the dQ/dV plots that the two pairs of reversible redox peaks do not change significantly, indicating that the structure remains stable upon cycling. This result is consistent with our previous *ex situ* XRD result.[11]

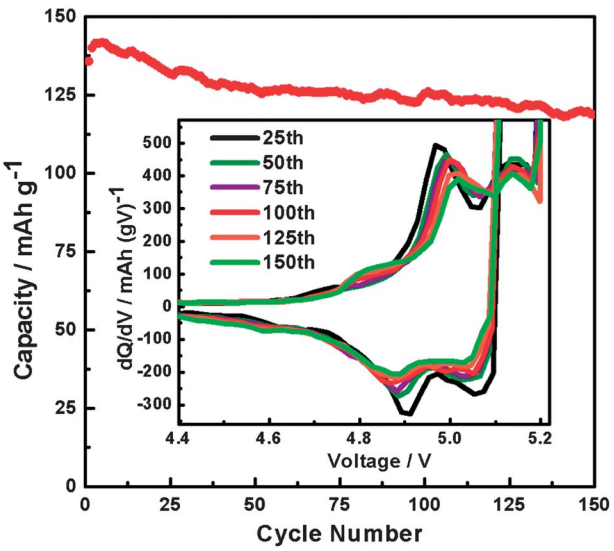

Fig. 9 Long-term cycling stability of the Li_3PO_4-coated Li_2CoPO_4F in the electrolyte with LiBOB additive. The inset is the corresponding dQ/dV *versus* voltage plots at different cycles. The voltage range is 2–5.2 V. The current density is 143 mA g^{-1}.

Conclusions

In summary, we have successfully developed a sol–gel method to achieve *in situ* Li_3PO_4 coating on the surface of the Li_2CoPO_4F cathode material. This double-layer surface coating contributes greatly to the electrochemical properties of the material. The carbon in the outer layer facilitates the transport kinetics of electrons and inhibits the growth of particle sizes. The Li_3PO_4 in the inner layer eliminates the surface anisotropy of Li_2CoPO_4F and enhances the lithium ion diffusion kinetics. Moreover, the inert Li_3PO_4 reduces the contact area between the active material and the electrolyte, which significantly improves the cycling performance. The LiBOB electrolyte additive shows a synergistic effect with the Li_3PO_4 coating layer in further stabilizing the

electrode/electrolyte interface, and the stabilized interface can suppress the increase of charge transfer resistance upon cycling. A capacity of 119 mA h g^{-1} with 83.8% capacity retention after 150 cycles has been achieved for the Li_3PO_4-coated Li_2CoPO_4F sample. High capacity, high working voltage, excellent rate capability and impressive cycling performance demonstrate that Li_2CoPO_4F is a promising high energy density and high power density cathode material for Li-ion batteries with long term cycling performance.

Acknowledgements

Financial support from the National Basic Research Program of China (973 program, grant no. 2011CB935903) and the National Natural Science Foundation of China (grant no. 21233004 and 21021002) is gratefully acknowledged.

Notes and references

1 J. M. Tarascon, *Philos. Trans. R. Soc. London, Ser. A*, 2010, **368**, 3227–3241.
2 Z. Gong and Y. Yang, *Energy Environ. Sci.*, 2011, **4**, 3223–3242.
3 Y. U. Park, D. H. Seo, B. Kim, K. P. Hong, H. Kim, S. Lee, R. A. Shakoor, K. Miyasaka, J. M. Tarascon and K. Kang, *Sci. Rep.*, 2012, 2.
4 S. Okada, M. Ueno, Y. Uebou and J.-i. Yamaki, *J. Power Sources*, 2005, **146**, 565–569.
5 B. L. Ellis, W. R. M. Makahnouk, Y. Makimura, K. Toghill and L. F. Nazar, *Nat. Mater.*, 2007, **6**, 749–753.
6 B. L. Ellis, W. R. M. Makahnouk, W. N. Rowan-Weetaluktuk, D. H. Ryan and L. F. Nazar, *Chem. Mater.*, 2010, **22**, 1059–1070.
7 X. Wu, J. Zheng, Z. Gong and Y. Yang, *J. Mater. Chem.*, 2011, **21**, 18630–18637.
8 J. G. Yu, K. M. Rosso, J. G. Zhang and J. Liu, *J. Mater. Chem.*, 2011, **21**, 12054–12058.
9 S. Amaresh, G. J. Kim, K. Karthikeyan, V. Aravindan, K. Y. Chung, B. W. Cho and Y. S. Lee, *Phys. Chem. Chem. Phys.*, 2012.
10 N. V. Kosova, E. T. Devyatkina and A. B. Slobodyuk, *Solid State Ionics*, 2012, **225**, 570.
11 X. Wu, Z. Gong, S. Tan and Y. Yang, *J. Power Sources*, 2012, **220**, 122–129.
12 W. Xu, X. Chen, F. Ding, J. Xiao, D. Wang, A. Pan, J. Zheng, X. S. Li, A. B. Padmaperuma and J.-G. Zhang, *J. Power Sources*, 2012, **213**, 304–316.
13 K. Kiyoshi, *J. Power Sources*, 1999, **81–82**, 123–129.
14 Z. R. Zhang, H. S. Liu, Z. L. Gong and Y. Yang, *J. Electrochem. Soc.*, 2004, **151**, A599–A603.
15 J. M. Zheng, Z. R. Zhang, X. B. Wu, Z. X. Dong, Z. Zhu and Y. Yang, *J. Electrochem. Soc.*, 2008, **155**, A775–A782.
16 Y.-K. Sun, M.-J. Lee, C. S. Yoon, J. Hassoun, K. Amine and B. Scrosati, *Adv. Mater.*, 2012, **24**, 1192–1196.
17 J. Cho, Y.-W. Kim, B. Kim, J.-G. Lee and B. Park, *Angew. Chem., Int. Ed.*, 2003, **42**, 1618–1621.
18 Q. Y. Wang, J. Liu, A. V. Murugan and A. Manthiram, *J. Mater. Chem.*, 2009, **19**, 4965–4972.
19 J. Liu and A. Manthiram, *Chem. Mater.*, 2009, **21**, 1695–1707.
20 Y. Jin, N. Li, C. H. Chen and S. Q. Wei, *Electrochem. Solid-State Lett.*, 2006, **9**, A273–A276.
21 H. G. Song, J. Y. Kim, K. T. Kim and Y. J. Park, *J. Power Sources*, 2011, **196**, 6847–6855.
22 X. Li, R. Yang, B. Cheng, Q. Hao, H. Xu, J. Yang and Y. Qian, *Mater. Lett.*, 2012, **66**, 168–171.
23 Y. Zheng, S. Taminato, Y. Xu, K. Suzuki, K. Kim, M. Hirayama and R. Kanno, *J. Power Sources*, 2012, **208**, 447–451.
24 B. Kang and G. Ceder, *Nature*, 2009, **458**, 190–193.
25 K. Abe, K. Miyoshi, T. Hattori, Y. Ushigoe and H. Yoshitake, *J. Power Sources*, 2008, **184**, 449–455.
26 A. von Cresce and K. Xu, *J. Electrochem. Soc.*, 2011, **158**, A337–A342.
27 L. Yang, T. Markmaitree and B. L. Lucht, *J. Power Sources*, 2011, **196**, 2251–2254.
28 J. Liu, T. E. Conry, X. Song, L. Yang, M. M. Doeff and T. J. Richardson, *J. Mater. Chem.*, 2011, **21**, 9984–9987.
29 V. Aravindan, Y. L. Cheah, W. C. Ling and S. Madhavi, *J. Electrochem. Soc.*, 2012, **159**, A1435–A1439.
30 D. Wang, J. Xiao, W. Xu, Z. Nie, C. Wang, G. Graff and J.-G. Zhang, *J. Power Sources*, 2011, **196**, 2241–2245.
31 D. Y. Wang, J. Xiao, W. Xu, Z. M. Nie, C. M. Wang, G. Graff and J. G. Zhang, *J. Power Sources*, 2011, **196**, 2241–2245.
32 G. T.-K. Fey, P. Muralidharan, C.-Z. Lu and Y.-D. Cho, *Solid State Ionics*, 2005, **176**, 2759–2767.
33 S. H. Choi, J. H. Kim, Y. N. Ko, Y. J. Hong and Y. C. Kang, *J. Power Sources*, 2012, **210**, 110–115.
34 J. Chong, S. Xun, X. Song, G. Liu and V. S. Battaglia, *Nano Energy*, 2013, **2**, 283–293.
35 J. Zheng, J. Xiao, W. Xu, X. Chen, M. Gu, X. Li and J.-G. Zhang, *J. Power Sources*, 2013, **227**, 211–217.
36 S. Dalavi, M. Xu, B. Knight and B. L. Lucht, *Electrochem. Solid-State Lett.*, 2012, **15**, A28–A31.
37 B.-T. Yu, W.-H. Qiu, F.-S. Li and L. Cheng, *J. Power Sources*, 2007, **166**, 499–502.
38 S. Chattopadhyay, A. L. Lipson, H. J. Karmel, J. D. Emery, T. T. Fister, P. A. Fenter, M. C. Hersam and M. J. Bedzyk, *Chem. Mater.*, 2012, **24**, 3038.
39 D. Aurbach, K. Gamolsky, B. Markovsky, G. Salitra, Y. Gofer, U. Heider, R. Oesten and M. Schmidt, *J. Electrochem. Soc.*, 2000, **147**, 1322–1331.